Princeton Plasma Physics Laboratory

PPPL-5316

Error Field Measurement, Correction and Heat Flux Balancing on Wendelstein 7-X

S. Lazerson, D. Gates

October 2016

Prepared for the U.S. Department of Energy under Contract DE-AC02-09CH11466.

Princeton Plasma Physics Laboratory
Report Disclaimers

Full Legal Disclaimer

Trademark Disclaimer

PPPL Report Availability

Princeton Plasma Physics Laboratory:

http://www.pppl.gov/techreports.cfm

Office of Scientific and Technical Information (OSTI):

http://www.osti.gov/scitech/

Related Links:

U.S. Department of Energy

U.S. Department of Energy Office of Science

U.S. Department of Energy Office of Fusion Energy Sciences

Error field measurement, correction and heat flux balancing on Wendelstein 7-X ‡

Samuel A. Lazerson[1], Matthias Otte[2], Marcin Jakubowski[2], Ben Israeli[3], Glen A. Wurden[4], Uwe Wenzel[2], Tamara Andreeva[2], Sergey Bozhenkov[2], Christoph Biedermann[2], Gábor Kocsis[5], Tamás Szepesi[5], Joachim Geiger[2], Thomas Sunn Pedersen[2], David Gates[1] and the W7-X Team

[1]Princeton Plasma Physics Laboratory, Princeton NJ, 08543, USA
[2]Max-Planck-Institut für Plasmaphysik, 17491, Greifswald, Germany
[3]Columbia University, New York NY, 10027, USA
[4]Los Alamos National Laboratory, Los Alamos, NM, 87545, USA
[5]Wigner Research Center for Physics, Budapest, Hungary

E-mail: lazerson@pppl.gov

Abstract. The measurement and correction of error fields in Wendelstein 7-X (W7-X) is critical to long pulse high beta operation, as small error fields may cause overloading of divertor plates in some configurations. Accordingly, as part of a broad collaborative effort, the detection and correction of error fields on the W7-X experiment has been performed using the trim coil system in conjunction with the flux surface mapping diagnostic and high resolution infrared camera . In the early commissioning phase of the experiment, the trim coils were used to open an n/m=1/2 island chain in a specially designed magnetic configuration. The flux surfacing mapping diagnostic was then able to directly image the magnetic topology of the experiment, allowing the inference of a small ~ 4 *cm* intrinsic island chain. The suspected main sources of the error field, slight misalignment and deformations of the superconducting coils, are then confirmed through experimental modeling using the detailed measurements of the coil positions. Observations of the limiters temperatures in module 5 shows a clear dependence of the limiter heat flux pattern as the perturbing fields are rotated. Plasma experiments without applied correcting fields show a significant asymmetry in neutral pressure (centered in module 4) and light emission (visible, H-alpha, CII, and CIII). Such pressure asymmetry is associated with plasma-wall (limiter) interaction asymmetries between the modules. Application of trim coil fields with n=1 waveform correct the imbalance. Confirmation of the error fields allows the assessment of magnetic fields which resonate with the n/m=5/5 island chain.

PACS numbers: 52.55.Hc,52.70.Kz

1. Introduction

The detection and compensation of error fields is of critical importance in all magnetically confined fusion devices, with the Wendelstein 7-X (W7-X) experiment being no exception [1, 2]. Achieving the key goals of the W7-X experiment, namely 30 minutes discharges at 5% plasma beta and reactor relevant triple product, will require careful control of the magnetic configuration [3]. This is because in a stellarator the vast majority of the confining magnetic field comes from the magnetic coils. This provides an inherently steady-state configuration, and allows the tailoring of confinement through shaping of the magnetic field [4]. However, unintended sources of magnetic fields can spoil confinement in a variety of ways. The most common pathway to degraded confinement is through the formation of magnetic islands. Here flux surfaces with low order rationality in their rotational transform can form into magnetic islands (thus spoiling confinement). This happens when magnetic fields which resonate with those surfaces are present. This is avoided in W7-X through the development of a magnetic configuration which avoids most low-order rationals in the confinement region. However, the divertor configuration of W7-X relies on an $n/m = 5/5$ island chain at the plasma edge. If uncompensated error fields in the device resonate with this island chain (in particular the $n/m = 1/1$ fields), the five fold stellarator symmetry of the device can be broken. Overloading of the divertor plates then limits plasma performance at even modest levels of error fields. Thus the detection and correction of error fields has played an important role in the first operational campaign (OP1.1) of W7-X.

Experiments to detect and correct error fields during the OP1.1 campaign made extensive use of the trim coil system [5, 6]. Each of the five modules of W7-X are equipped with large water-cooled copper widow-pane style coils, located outside the cryostat. This system was used to produce both perturbing and compensating magnetic fields. During the flux surface mapping campaign they were used to generate an $n/m = 1/2$ island chain, allowing the presence of error fields to be detected through changes in the magnetic topology of the field lines [7]. A series of plasma discharges exploring limiter heat loads were also performed. Here a high resolution infrared camera [8, 9] provided detailed imaging of the limiter temperatures as an $n = 1$ magnetic perturbation was rotated. Compensation experiments were limited due to diagnostic coverage in the first campaign. However, the trim coils were able to symmetrize a neutral pressure anomaly detected between device sectors [10]. These experiments allow characterization of the error fields in W7-X during the first experimental campaign.

The possible sources of error fields are various (elastic deformations, construction mis-alignments, bus-bars, ferritic material, etc.) however those coming from magnetic coil misalignments and manufacturing deviations can be assessed in a direct manner. Detailed metrology of the superconducting coil set on W7-X allows simulation of these error fields [11, 12, 13]. Each coil case has been measured at 768 points (and several alignment reference marks) to provide such a model. This model was analyzed to include the effects of pre-loading, dead-weight, thermal contraction, and electromagnetic

loads. The resulting coil geometry can be fed into field line tracing software to provide comparison with experimental measures. In section 2, the experimental results regarding error fields are reviewed. In section 3, the modeling of the deformed coil geometry is presented and compared to experimental measures. In the final section these results are discussed and predictions for OP1.2 are made.

2. Measurements

2.1. The Compass Scan Technique

In this work, an experimental technique (colloquially known as a 'compass scan') has been employed to measure the effect of intrinsic error fields without directly measuring such fields (or their effects). In this technique a probing magnetic field of known phase and amplitude is applied to the experiment. As the magnetic field is composed of a linear superposition of magnetic fields, the experiment will respond to both the applied perturbing field and the intrinsic error field [14]. By varying the phase and amplitude of the probing field, the response of other quantities in the device (which are sensitive to these magnetic fields) are measured. The dependence of the measured quantity on the phase and amplitude of the applied error field can then be constructed. Should no intrinsic error field exist, this dependence should be centered on the zero amplitude point of the applied field phase and amplitude scan. If the dependence is centered elsewhere then the intrinsic error field has been detected. The offset from zero provides the phase and amplitude of the intrinsic error field. Figure 1 provides a schematic depiction of this method.

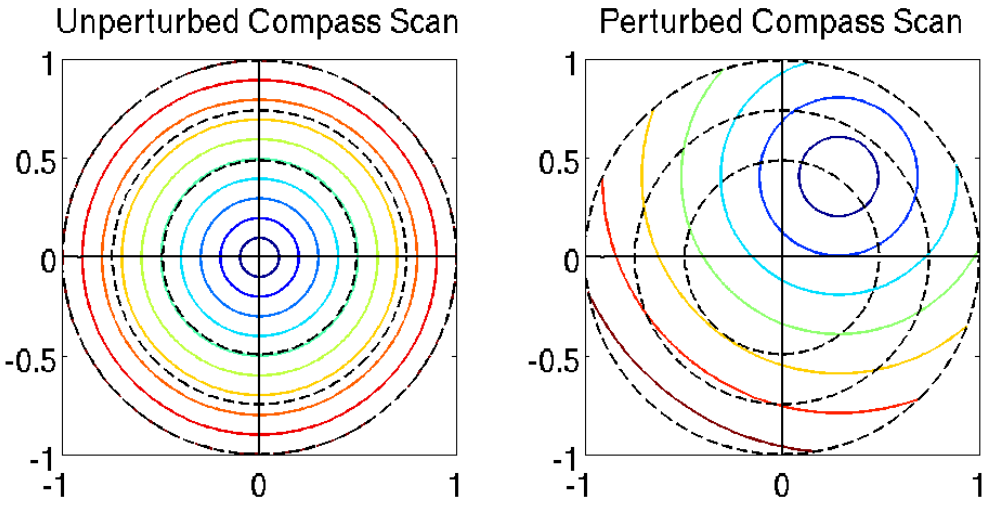

Figure 1. Cartoon example of a compass scan showing the unperturbed (left) and perturbed configuration (right). Color contours indicate diagnostic response, showing a minima at 55^o and approximately half amplitude for the perturbed case (right). Here perturbed refers to the existence of an error field and the axis are normalized to the maximum applied field.

In the W7-X experiment the trim coil system provides the probing magnetic field. As error fields with $n = 1$ behavior are of interest, these coils are energized with an $n = 1$ pattern. No direct poloidal mode control is possible with this coil set. During the flux surface mapping experiments an $\iota = n/m = 1/2$ surface was used to image an $m = 2$ island chain. The width of the island lobes provided a quantity to measure and map to the applied field phase and amplitude. The limiter tile temperatures provided a similar quantity during plasma operation. In this way, the 'compass scan' technique was used to measure error fields during the first operational campaign of W7-X.

2.2. Flux Surface Mapping

The first evidence of the presence of error fields was detected during the flux surface mapping experiments in W7-X. A $n/m = 5/6$ intrinsic island chain was imaged in the limiter magnetic configuration [15]. The presence of this island chain was expected and its radial motion with toroidal field strength confirms that the magnets are undergoing elastic deformation due to electromagnetic forces. A small $n/m = 4/5$ island chain was also detected. This island chain was not expected and suggests that error fields with resonant harmonics indeed do exist in the device.

The presence of error fields in W7-X was directly addressed by the flux surface mapping technique through the $\iota = 1/2$ magnetic configuration [7]. In this configuration, the $\iota = 1/2$ rational surface is placed at the mid-radius of the confinement region. Should the coils not be deformed, and no other sources of magnetic field present, there would be a vanishingly small $n/m = 5/10$ island chain. In the experiment, emitter shadowing prevented the direct imaging of this region. However, using the trim coil system to perform a 'compass scan,' a large $n/m = 1/2$ island chain was opened. From this work a small ~ 4 *cm* intrinsic island chain was determined to be present. The phase of this error field was also determined in that work.

The experiment was unable to directly address the $n/m = 1/1$ error field in the first experimental campaign. This was due to administrative and technical limits on coil currents during the first experimental campaign. Specifically, the high-iota configuration (in which $iota \sim 1$ on axis) requires the reversal of the planar superconducting coil currents. Examination of the magnetic axis excursion from the mid plane of the device should provide information on this component of the error field. This is important as compensation of the $n/m = 1/1$ error field is essential to high performance divertor operation in W7-X [2].

2.3. Limiter Temperatures

The effect of error fields on plasma performance was examined during plasma operation in the first experimental campaign. A series of discharges with applied $n = 1$ trim coil fields were performed. In these discharges the phase and amplitude of the field were varied in order to perform a 'compass scan.' Figure 2 depicts a typical limiter IR camera image [8, 9] and the dependence of the peak temperature on applied trim coil field. The

lines across which the limiter temperature are being analyzed have been depicted in the image. Peak values on the left and right side of the image are plotted. A peak in the temperatures around 90^o applied trim coil phase is in qualitative agreement with flux surface mapping results (135^o). Specifically the peaking of the temperature falls in the direction of module two ($72^o - 144^o$). This suggests that at this point the applied trim coil field was aligned with the intrinsic error field. The quantitative disagreement can be attributed to coil deformations due to differences in field strength and possible misalignment of the limiters themselves. The $m/n = 2/1$ error field was measured at $\sim 0.3\ T$ while these measurements were performed at $\sim 2.5\ T$. Analysis of the effect of amplitude variation was inconclusive due to deteriorating plasma performance.

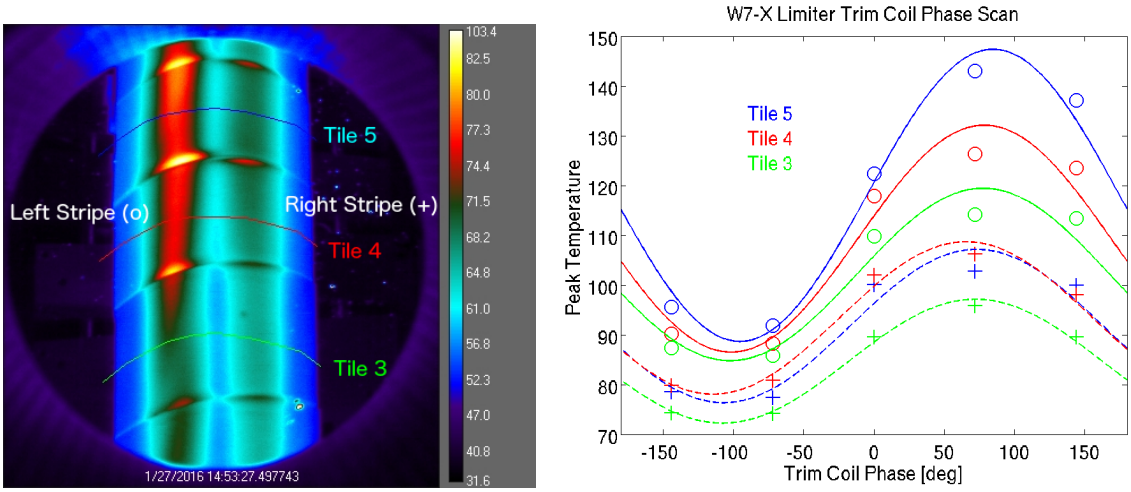

Figure 2. Limiter IR camera image (left) and dependence of limiter temperatures on applied trim coil phase at 1000 A (right). Temperatures on the left hand side (o) and right hand side (+) are plotted, along with $n = 1$ fits to the data.

2.4. Neutral pressure symmetrization

The ability of the trim coils to compensate asymmetries was demonstrated using the neutral pressure manometer system on W7-X [10]. In this system, the neutral pressure could be measured in four of the five modules. A discrepancy in the neutral pressure measured in module four was identified early in the experimental campaign. It has been consistently observed that the increased pressure in module four lead to radiation collapse and shorter plasma durration. The neutral pressure serves as a proxy for the plasma-wall interaction. It was discovered that this asymmetry had a functional dependence on the applied trim coil $n = 1$ field (while conducting the experiments of the previous section). Figure 3 demonstrates this dependence. This figure shows that the neutral pressures could be symmetrized between modules if the field was aligned in the -72^o direction. This is approximately the opposite direction of the error field phase as determined by limiter plasma experiments and the flux surface mapping campaign.

Thus further confirming the error field measurements.

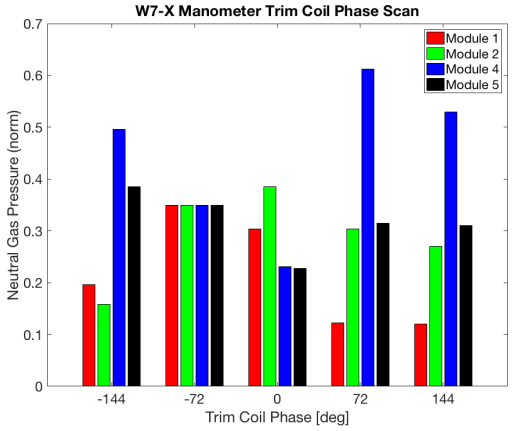

Figure 3. Dependence of manometer pressures as a function of applied trim coil $n = 1$ magnetic field phase. Symmetrization is present for a phase in agreement with predicted phase of the error field. All runs performed at 1000 A peak coil current.

3. Modeling

It is theorized that small symmetry breaking deviations in the superconducting coil set are responsible for the observed error fields in this first experimental campaign. Using detailed measurements of the coil positions and numerical analysis of coil structural loading, this hypothesis can be verified. Once verified, these coil models can be used to predict the effects of such loading on future experiments.

3.1. The W7-X Superconducting Coil Set

The superconducting coil set of one half module of W7-X is composed of five unique non-planar coils and two planar coils [16]. This set of coils mirrors across a field period, producing stellarator-symmetry. Accounting for all five field periods, the device has 70 superconducting modular coils. The coils themselves have slight manufacturing deviations which would alone produce error fields [12, 13]. To compensate for these deviations, the coils have been repositioned (relative to design specifications) in an attempt to minimize the unwanted $n/m = 1/1$ component of the error field. Additionally, the weight of the coils, cooling, and electromagnetic loads create elastic deformations of the superconducting coils. Using the detailed measurements of coil positions after installation and load analysis coil models have been developed which can be used in field line tracing simulations.

In this work we refer to 'CAD' and 'as-built' coil models, along with an 'FEM' modifier. The 'CAD' label refers to the ideal design specification coil. Such a coil should produce no fields with toroidal mode number less than 5, owing to stellarator symmetry.

The 'as-built' coil refers to the coil as it was measured after construction. Such measurements were made at room temperature. The 'FEM' (finite element modeling) modifier implies that the initial positions have been used and dead-weight, cool-down, pre-load, and electromagnetic loads have been accounted for. Thus this modifier can be used with 'CAD' and 'as-built' models. These models are interfaced to the FIELDLINES code, a versatile field line tracing code.

3.2. The Intrinsic Error Field

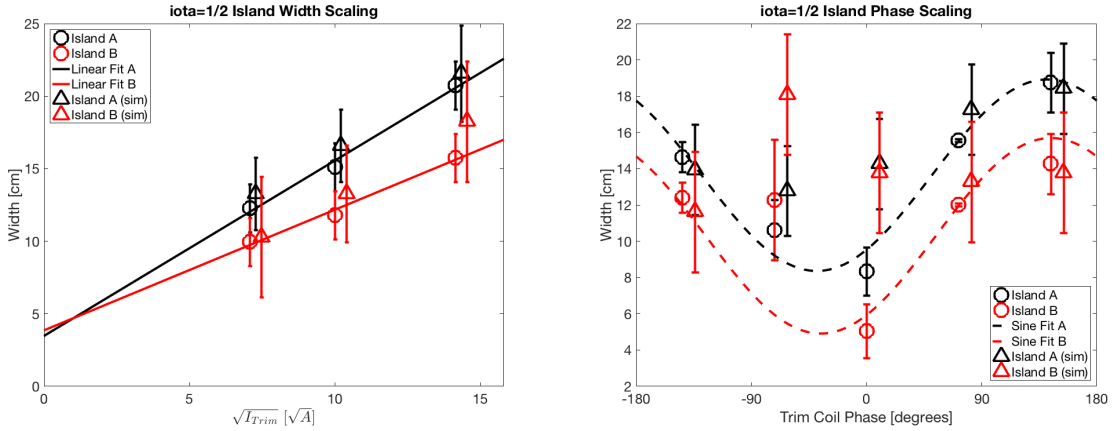

Figure 4. Simulated (triangle) and experimental (o) data for trim coil amplitude and phase scans. Simulations were preformed using the 'as-built' W7-X coil set. Simulated data points have been shifted right slightly to aid in visualization. The abscissa in the left hand plot is the theoretical scaling of island width ($\sqrt{I_{Trim}}$).

In order to confirm the source of the $n/m = 1/2$ error field simulations using the various coil sets were performed. The 'CAD' coil set indicated no island chain at the $n/m = 1/2$ rational surface when performing a simulated flux surface mapping. Poincaré plots suggested a vanishing small $n/m = 5/10$ island chain for this coil model. Application of trim coil fields to the 'CAD' model indicated that island widths should scale as $\sqrt{I_{trim}}$, in agreement with theory [17]. Phase scan also found no offset in the island widths (as expected). Modeling with the 'as-built' coil set told a different story. Poincaré plots using this coil confirmed the presence of an $n/m = 1/2$ island chain, whose width was approximately 4 *cm*. Figure 4 depicts the results of simulated flux surface mappings alongside the previously published experimental analysis. Effort was made to mimic the emitter positions used in the experiment. The agreement between experimental measurements and simulated measurements appears excellent. Simulation and measurement agree on the extrapolation to a 4 *cm* intrinsic island width. The phase scan also appears fairly consistent with experiment.

In the analysis of the $\iota = 1/2$ configuration the 'FEM' analysis was neglected. The justification for this primarily relies on the fact that these experiments were conducted at low field ($\sim 0.3\ T$). Thus electromagnetic loads should be negligible. It in turn allows

us to confirm the position of the coils as being the source of any error field, validating the 'as-built' coil model for additional 'FEM' analysis. Neglect of the electromagnetic loading caused by the trim coils themselves may account for the discrepancies seen at trim coil phase -72^o and 0^o.

3.3. Field strength dependency

The effect of electromagnetic loads on magnetic configuration was evident in flux surface mappings of the OP1.1 limiter configuration. In these experiments a radial shift in the $n/m = 5/6$ island chain was present as the toroidal field was ramped up. Comparison with the 'CAD-FEM' models provided qualitative agreement but not quantitative agreement. In particular, the best fit to flux surface images was found for electromagnetic loads $\sim 60\%$ the actual experimental values. In this work the fit was performed using the first five passes of the electron beam. This also confirms that the 'CAD' coil was not sufficient for this analysis.

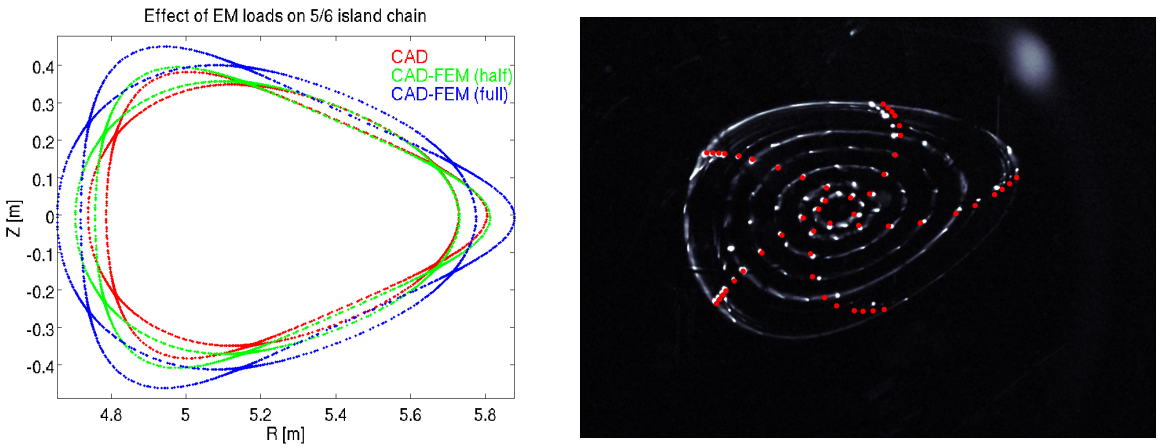

Figure 5. Simulations showing the change in 5/6 island position with field strength (left) and best fit of simulation results to experiment (right). Simulations were performed using the 'CAD' coil model at zero, half field, and full field strength (2.5 T). Best fit found for 1.9 T FEM model using first five electron beam passes.

3.4. Effect on limiters

The distribution of connection lengths on the limiter surface served as a proxy for heat deposition patterns in previous simulations [18]. Figure 6 shows the connections lengths between the limiters using the 'CAD' coil model. Three distinct regions are clearly visible in the plot. Field lines in the upper region (marked by the blue circle) traverse one full transit of the torus before landing on the toroidally adjacent limiter (blue trace). Field lines in the lower region (marked by the green circle) map back to the limiter from which they start after one toroidal transit (green trace). The field lines in the deposition region (marked by the red circle) make two toroidal transits before

landing on the adjacent limiter. We call these regions the deposition regions as the temperature peaks on the limiters appear to correlate well with these features. The extremely long connection lengths seen at the edges of the panel are artifacts of the integration step size, as are the jaggedness of the plot near the edge.

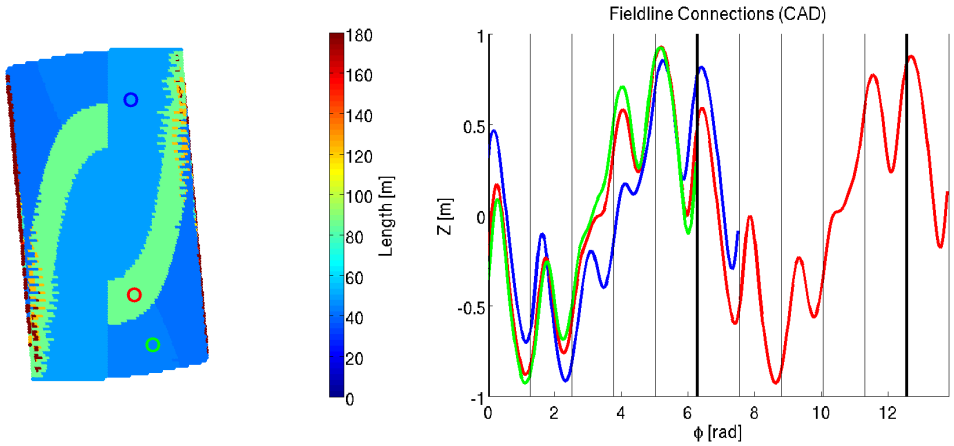

Figure 6. Limiter connection lengths for the 'CAD' coil model (left) and field line traces for three select regions (right). The connection length plot (left) has circle indicating start positions of field lines (the projection is in vertical distance and toroidal angle). In the field line trace (right) thin lines indicate limiters and thick lines indicate the module one limiter.

Using the 'as-built-FEM' coil model the connection lengths for the limiters were again analyzed (figure 7). While the generic features of the 'CAD' coil model persist, new features appear which suggest the possibility of heat load asymmetries between divertor modules. Most striking are features near the top and bottom of most limiters. In these regions the connection lengths appear to become much longer (limiters two and four). Additionally, a feature near the center of the limiter appears on limiters four and one. These features appear to have the same connection length as the deposition region. This suggests the possibility of additional regions of limiter heat loading.

4. Discussion

The studies of error fields in W7-X performed during the first experimental campaign paint a consistent picture of error fields and their sources in the device. Flux surface mapping, limiter temperatures, and neutral pressure measurements depict a consistent picture of the phase of an $n = 1$ error field. Detailed analysis of flux surface imaging campaign confirms the source of the error fields to be due to slight misalignments of the superconducting magnetic coils. Moreover, these measurements indicate the necessity of mechanical, thermal and electromagnetic load modeling, for accurate depiction of the magnetic field. So while care must be taken in the modeling of these fields, they are well within the capabilities of the trim coils system in terms of compensation.

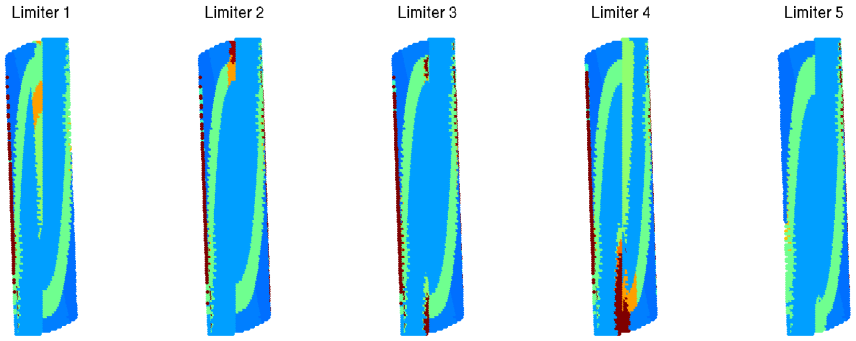

Figure 7. Limiter connection lengths for the 'as-built-FEM' coil model for all five limiters. Notice that features have appeared at the top and bottom of most limiters. Color scale is the same as in figure 6.

Looking forward to the next operational campaign, we can now predict with some confidence the role error fields will play. In OP1.1 we were not able to directly measure the $n/m = 1/1$ component of the magnetic field. This will be done in OP1.2 using the 'high-iota' configuration. The 'compass-scan' technique will be used to analyze the helical shift of the W7-X magnetic axis in this configuration. However, the results obtained here already provide confidence that the trim coils will be capable of symmetrizing divertor mis-loading between modules.

Acknowledgments

The authors would like to thank the referees for their insightful remarks and someone else.

B. Israeli would like to thank the US DOE Summer Undergraduate Laboratory Internship (SULI) program for funding his contribution to this work.

This work has been carried out within the framework of the EUROfusion Consortium and has received funding from the Euratom research and training programme 2014-2018 under grant agreement No 633053. The views and opinions expressed herein do not necessarily reflect those of the European Commission.

[1] Sergey A Bozhenkov, Joachim Geiger, M Grahl, Johann Kisslinger, A Werner, and R C Wolf. Service oriented architecture for scientific analysis at W7-X. An example of a field line tracer. *Fusion Engineering and Design*, 88(11):2997–3006, November 2013.

[2] Sergey A Bozhenkov, Samuel Lazerson, Matthias Otte, David A Gates, T Sunn Pedersen, and R C Wolf. Methods for measuring 1/1 error field in Wendelstein 7-X stellarator. *Nuclear Fusion*, page 076002, June 2016.

[3] Joachim Geiger, Craig D Beidler, Y Feng, Henning Maaßberg, N B Marushchenko, and Y Turkin. Physics in the magnetic configuration space of W7-X. *Plasma Physics and Controlled Fusion*, pages 1–11, November 2014.

[4] H E Mynick. Transport optimization in stellarators. *Physics of Plasmas*, 13(5):058102, 2006.

[5] Thomas Rummel, Konrad Rieße, Frank Fullenbach, Matthias Koppen, Johann Kisslinger, Tom Brown, Ron Hatcher, Stephen Langish, Mike Mardenfeld, and George Hutch Neilson. The

Wendelstein 7-X Trim Coil System. *IEEE Transactions on Applied Superconductivity*, 24(3):1–4, 2014.

[6] T Rummel, K Risse, Johann Kisslinger, M Köppen, F Fullenbach, George Hutch Neilson, Thomas Brown, and S Ramakrishnan. The Trim Coils for the Wendelstein 7-X Magnet System. *IEEE Transactions on Applied Superconductivity*, 22(3):4201704–4201704, 2012.

[7] Samuel Lazerson, Matthias Otte, Sergey Bozhenkov, Christoph Biedermann, Thomas Sunn Pedersen, and the W7-X Team. First measurements of error fields on W7-X using flux surface mapping. *Nuclear Fusion*, page 106005, August 2016.

[8] G A Wurden, L A Stephey, C Biedermann, M W Jakubowski, J P Dunn, M Gamradt, and W7-X Team. A high resolution IR/visible imaging system for the W7-X limiter. *Review of Scientific Instruments*, 87(11):11D607, August 2016.

[9] L Stephey, G A Wurden, O Schmitz, H Frerichs, F Effenberg, C Biedermann, J Harris, R König, P Kornejew, M Krychowiak, E A Unterberg, and W7-X Team. Spectroscopic imaging of limiter heat and particle fluxes and the resulting impurity sources during Wendelstein 7-X startup plasmas. *Review of Scientific Instruments*, 87(11):11D606, August 2016.

[10] Maciej Krychowiak and et al. Overview of diagnostic performance and results for the first operation phase in wendelstein 7-x. Submitted, 2016.

[11] T. Andreeva, T. Bruer, V. Bykov, K. Egorov, M. Endler, J. Fellinger, J. Kilinger, M. Kppen, and F. Schauer. Tracking of the magnet system geometry during wendelstein 7-x construction to achieve the designed magnetic field. *Nuclear Fusion*, 55(6):063025, 2015.

[12] T Andreeva, T Bräuer, M Endler, Johann Kisslinger, and Y Igitkhanov. Analysis of the magnetic field perturbations during the assembly of Wendelstein 7-X. *Fusion Science and Technology*, 46(2):388–394, September 2004.

[13] T Andreeva, T Bräuer, M Endler, Johann Kisslinger, and U v Toussaint. Influence of construction errors on Wendelstein 7-X magnetic configurations. *Fusion Engineering and Design*, 84(2-6):408–412, June 2009.

[14] R J Buttery, A H Boozer, Y Q Liu, J K Park, N M Ferraro, V Amoskov, Y Gribov, R J La Haye, E Lamzin, J E Menard, Michael J Schaffer, E J Strait, and the DIII-D Team. The limits and challenges of error field correction for ITER. *Physics of Plasmas*, 19(5):056111, 2012.

[15] Matthias Otte, D Aßmus, C Biedermann, Sergey A Bozhenkov, T Bräuer, A Dudek, Joachim Geiger, G Kocsis, Samuel Lazerson, T S Pedersen, F Schauer, T Szepesi, B Standley, and the W7-X Team. Setup and initial results from the magneticflux surface diagnostics at Wendelstein 7-X. *Plasma Physics and Controlled Fusion*, page 064003, May 2016.

[16] Thomas Rummel, Konrad Rieße, Gunnar Ehrke, Kerstin Rummel, Andre John, Thomas Monnich, Klaus-Peter Buscher, Walter H Fietz, Reinhard Heller, Olaf Neubauer, and Anatoly Panin. The Superconducting Magnet System of the Stellarator Wendelstein 7-X. *IEEE Transactions on Plasma Science*, 40(3):769–776, 2012.

[17] Allen H Boozer. Physics of magnetically confined plasmas. *Rev.Mod.Phys.*, 76:1071–1141, 2004.

[18] Thomas Sunn Pedersen, T Andreeva, H S Bosch, Sergey A Bozhenkov, F Effenberg, M Endler, Y Feng, David A Gates, Joachim Geiger, D Hartmann, H Hölbe, M Jakubowski, R König, H P Laqua, Samuel Lazerson, Matthias Otte, M Preynas, O Schmitz, T Stange, Y Turkin, and the W7-X Team. Plans for the first plasma operation of Wendelstein 7-X. *Nuclear Fusion*, pages 1–13, November 2015.

PPPL PRINCETON PLASMA PHYSICS LABORATORY

Princeton Plasma Physics Laboratory
Office of Reports and Publications

Managed by
Princeton University

under contract with the
U.S. Department of Energy
(DE-AC02-09CH11466)

P.O. Box 451, Princeton, NJ 08543
Phone: 609-243-2245
Fax: 609-243-2751

E-mail: publications@pppl.gov

Website: http://www.pppl.gov